Open Access

*Catalysis Research*

LIDSEN Publishing Inc.

Original Research

# A Remarkable Pt Doped CNT Catalyst as a Double Functional Material: Its Application for Hydrogen Production and Supercapacitor

Tülin Avcı Hansu *

Faculty of Engineering, Department of Chemical Engineering, Siirt University, Siirt 56100, Turkey; E-Mails: tulinn_avci@hotmail.com; tulin.hansu@siirt.edu.tr

* **Correspondence:** Tülin Avcı Hansu; E-Mails: tulinn_avci@hotmail.com; tulin.hansu@siirt.edu.tr

**Academic Editor:** Wei Wang

**Special Issue**: Recent Advances in Pt-Based Catalysts

*Catalysis Research*
2024, volume 4, issue 2
doi:10.21926/cr.2402005

**Received:** December 25, 2023
**Accepted:** May 08, 2024
**Published:** May 11, 2024

**Abstract**

In this study, by producing bifunctional material, hydrolysis, and supercapacitor applications were investigated. The carbon nanotube-supported Pt catalyst was prepared using the sodium borohydride ($NaBH_4$) reduction. Surface characterization of the synthesized Pt/CNT catalyst was performed using scanning electron microscopy-energy dıstrıbutıon X-ray spectrometer (SEM-EDX), X-ray diffraction (XRD), and transmission electron microscopy (TEM). Hydrolysis experiments were performed after deciding on the appropriate atomic ratio from the Pt/CNT catalysts synthesized in different nuclear ratios. The parameters affecting the hydrogen production from $NaBH_4$ were examined. As a result of the kinetic calculations, the initial rates of reaction for 30°C and 60°C were calculated as 21949,69 $mlH_2g_{cat}min^{-1}$ and 70018,18 $mlH_2g_{cat}min^{-1}$. Galvastonic charge-discharge (GCD), cyclic voltammetry (CV), and electrochemical impedance spectroscopy (EIS) were used as characterization techniques for the use of Pt/CNT catalysts as electrodes in supercapacitor applications. The specific capacitance value of 7% Pt/CNT catalyst at 1 A/g current density was calculated as 57,78 F/g. Energy and power density were calculated as 8,025 Wh/kg and 963 W/kg, respectively. Therefore, this catalyst is called a "cap-cat" with capacitor properties. The catalyst used in this study is promising for this recently studied topic.

**Keywords**
Bifunctional material; supercapacitor; hydrogen generation; catalyst; sodium borohydride

## 1. Introduction

Energy needs in the world are increasing rapidly with population growth and industrialization. Despite the increasing energy need, there has been no decrease in the use of fossil fuels, which are the world's primary energy source. Significant climate change has also caused a reduction in available resources [1, 2]. However, the leading cause of climate change is greenhouse gas emissions, especially $CO_2$, resulting from fossil use [3]. Hydrogen ($H_2$), a form of renewable energy, is universally accepted as a secondary clean energy source. So, hydrogen is an energy vector. Hydrogen as a fuel can help minimize greenhouse gas emissions, smoke, and acid rain because hydrogen only needs oxygen, and the only product formed from combustion is water [4-7]. However, since $H_2$ is not found in molecular form in nature, it must be produced and stored before use. Supercapacitors, used in energy storage, are also used to store the produced hydrogen. Supercapacitors have many uses due to their high safety, cost-effectiveness, fast charging, environmental friendliness, long cycle life, and operation in a wide temperature range. In addition, supercapacitors act as supporting systems in portable electronic devices, renewable energy generation technologies, and energy storage [8, 9]. Electric double-layer capacitors (EDLC) and so-called capacitors are the two forms of supercapacitors [10]. The energy storage mechanism is used to make this differentiation. The energy in electrical double-layer capacitors comes from the electrostatic storage of charges at the electrode-electrolyte interface [11, 12]. Nanostructured carbon-based electrode material is the most commonly utilized for electrochemical applications because of its low cost, superior electrical properties, and thermal and chemical durability [13]. Researchers have concentrated on this problem since developing next-generation electrodes and electrolytes to manufacture supercapacitors with high-energy storage capabilities is critical. For EDLC (electrical double layer capacitors) supercapacitors, specific capacitance in the range of 40-300 F/g has been described in the literature [14].

Chemical hydrogen storage materials such as $NaBH_4$ [15], $KBH_4$, $LiBH_4$ [16], and $NH_3BH_3$ [17] for hydrogen storage and transport can be called alternative compounds to produce $H_2$. Among hydrides as a promising hydrogen storage material, producing high-purity $H_2$ from $NaBH_4$ is popular because it has a 10.8% $H_2$ storage capacity by weight. Sodium borohydride ($NaBH_4$) has superior properties such as stability, low cost, non-flammability, non-toxic, controllable hydrolysis reaction, environmentally friendly, by-product reusability and highly soluble in water [18, 19]. Hydrogen attracts researchers' attention due to its properties. There are many studies on the storage and production of hydrogen in the literature. Researchers studied hydrogen production from $NaBH_4$ in the presence of designed catalysts [20-25] and the use of catalysts both in hydrogen production and as electrode material [9, 26-30]. In hydrogen production from $NaBH_4$, using catalysts from precious metals is quite common [31-33]. In manufacturing precious metal catalysts, reducing the quantity and overall cost is essential while maintaining the catalyst's effectiveness. For this, increasing the catalyst's surface area and the metal particles' dispersion is necessary using a support material [34]. Pt/CNT is one of the best catalysts for producing $H_2$ from $NaBH_4$. The amount of Pt in the catalyst

affects the reaction because the activated carbon domain support for Pt has a high surface area and stability [18]. The scarcity of Pt resources limits the application of Pt-based materials in the industry. Therefore, the mass-specific activity of Pt needs to be maximized as much as possible [35].

The primary purpose of this study is to show the use of Pt/CNT catalyst in hydrogen production and its use as electrode material for supercapacitor applications. The most promising electrocatalysts are still carbon-supported platinum (Pt/C) [36, 37]. In the literature review, catalysts consisting of CNT-supported Pt nanoparticles were studied [38-42]. Considering these studies, the study was started. In addition, this study's primary purpose is to show the hydrolysis and supercapacitor properties of the same catalyst. We have successfully achieved our goal with experimental studies. In the literature, electrooxidation, and supercapacitor properties of the obtained catalyst are emphasized, while in this study, hydrolysis and supercapacitor properties are emphasized, unlike the literature. Researchers have also reported the capacitor properties of the materials with catalyst properties [8, 27, 28, 41-43], characterizing them as capacitor-capable catalysts, "cap-cat". Here, catalysts were obtained by loading different amounts of Pt on the carbon nanotube support material. After selecting the catalyst suitable for hydrolysis, its supercapacitor property was examined. The supercapacitor property of the Pt/CNT catalyst was determined by cyclic voltammetry (CV), electrochemical impedance spectroscopy (EIS), and galvanostatic charge-discharge (GCD) electrochemical measurements. NaOH mass, $NaBH_4$ mass, catalyst amount, and temperature, the hydrolysis parameters, were examined.

## 2. Material and Method

### *2.1 Catalyst Preparation*

0.05 g of CNT was added to 10 ml of distilled water. The prepared solution was left to be mixed in the stirrer with the help of a magnet. Then, metal loading was done, and 0.5%, 1%, 3%, 5%, 7%, 10%, and 20% Pt were added by weight. It was kept in an ultra-sonic water bath for 40 minutes in a mixer for 80 minutes. After mixing, the $NaBH_4$ solution was added to the metal-containing solution. Again, it was kept in a water bath for 20 minutes in a mixer for 40 minutes. Finally, the synthesized catalyst was filtered with the help of filter paper, and the sediment on the filter paper was left to dry in a vacuumed oven at 85°C for 12 hours. The dried catalyst was taken into a suitable container and stored in the experiments.

### *2.2 Physical Characterization*

TEM, XRD, and SEM-EDX characterization methods were used to obtain information about the surface structure, morphology, and composition of the synthesized catalyst. Persee XD Series X-ray diffractometer (XRD) with Cu K radiation (=1.54056) was used to examine the lattice structure. A FEI QUANTA 250 FEG scanning electron microscope was used to perform SEM-EDX experiments. The Zess Sigma 300 TEM determined these catalysts' shape and size distributions.

### *2.3 Supercapacitor Electrode Preparation and Electrochemical Characterization*

90% of the weight of the prepared Pt/CNT catalyst was weighed and thoroughly ground. Polyvinylidene fluoride (PVDF) (10 percent by weight) was used as a binder to maintain the materials linked to one another and the current collector. N-methyl-2-pyrrolidone was used to dissolve PVDF

in the mixture (NMP). To obtain an excellent homogeneous slurry, the mixture was placed in an ultrasonic bath for 10 minutes and agitated for 2 hours. A current collector made of nickel foam was employed, and the slurry was poured onto it. The electrodes were dried under vacuum at 80°C for 24 hours to eliminate NMP from the mix. In a sealed aluminum test apparatus, two identical electrodes of 15 mm diameter round form anode and cathode, paper of 24 mm diameter as a thin separator, and 6 M potassium hydroxide (KOH) as electrolyte solution were used to make a two-electrode cell configuration. Galvanostatic charge-discharge (GCD), cyclic voltammetry (CV), and electrochemical impedance spectroscopy (EIS) techniques were used to characterize the supercapacitor electrochemically at room temperature.

Energy and power densities are two essential parameters for evaluating the electrochemical performance of supercapacitors. The maximum energy and power density of a supercapacitor is calculated as [43]:

$$E(\mathrm{Wh/kg}) = CV^2/2 \tag{2.1}$$

$$P(\mathrm{W/kg}) = V^2/4R \tag{2.2}$$

The equivalent series resistance is *c* in the equation; specific capacity, *V*; working potential and *R*. The following equations are used to calculate the EDLC capacitance by CV analysis [44].

$$C = Q_t/2\Delta V \tag{2.3}$$

$$C_s = C/m \tag{2.4}$$

$Q_t$ is the integral area of the CV curve, $\Delta V$ is the potential difference, and m is the amount of active material at both electrodes. As a result of the GCD analysis, the specific capacitance of a supercapacitor can be calculated using equation 2.5.

$$C_s = (2 * i * \Delta t)/(m * \Delta V) \tag{2.5}$$

*i*; discharge current, $\Delta t$; discharge time, and *m*; the amount of active material on the surface of an electrode.

## 3. Results and Discussion

### *3.1 Characterization Results*

Figure 1 shows XRD patterns of Pt/CNT, revealing the diffraction peaks of both Pt and carbon. For the Pt/CNT catalyst, the diffraction peak at about 25.8° referred to the (0 0 2) plane of the carbon's hexagonal structure [39]. Planes of face-centered cubic (fcc) Pt (1 1 1), (2 0 0), (2 2 0), (3 1 1) and (2 2 2) for Pt/CNT was observed at 40°, 46.4°, 67.6°, 79.2° and 81.9°. These planes confirm that the formation of pure Pt is strengthened by a high degree of crystallization [45]. The crystal size of 7% Pt/CNT was calculated using the Scherrer equation and shown to be 4.42 nm.

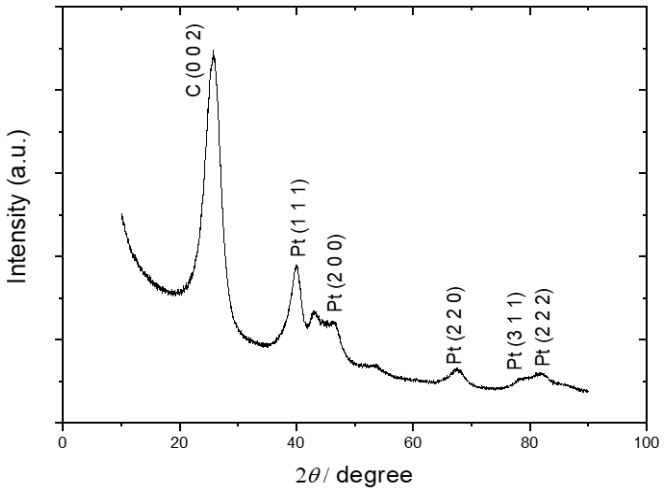


**Figure 1** XRD template of 7% Pt/CNT catalyst.

Figure 2(a-e) shows SEM-EDX and mapping images highlighting the formation and morphologies of the Pt/CNT catalyst. Figure 2(a, b) shows the carbon nanotube network and Pt. It was also observed that Pt metal settled in the tube. The dots appearing in white in the figure indicate that Pt metal is attached to the CNT surface. Moreover, the mapping image and elemental analysis results prove the attachment of Pt metal to CNT. The formation of the Pt/CNT catalyst was supported by the mapping analysis in which the turquoise and green particles exhibited Pt and carbon in Figure 2(c, d). The atomic and weight ratios of Pt and carbon elements from the EDX results are given in Table 1. Pt metal was obtained in the appropriate ratio on the carbon surface, as shown in the table.

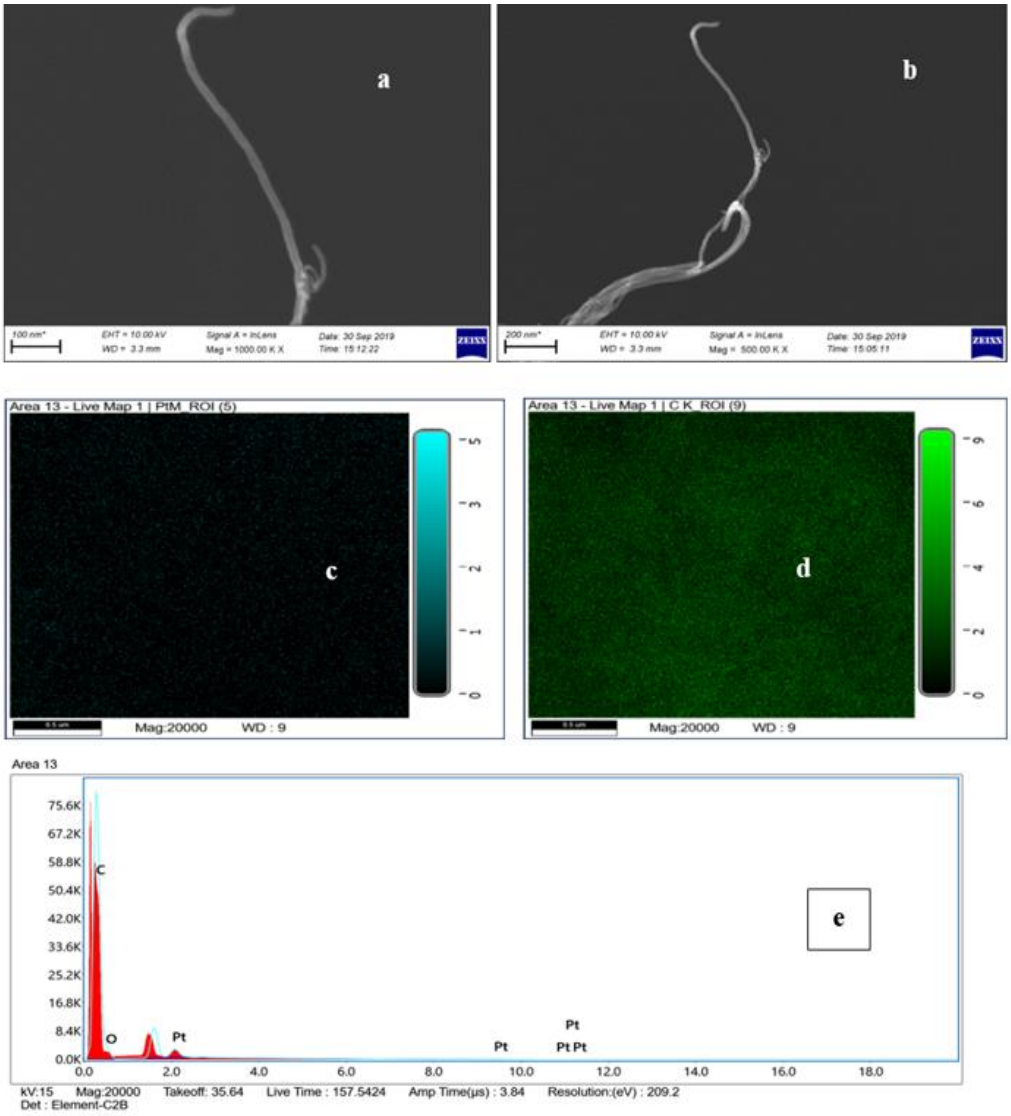


**Figure 2** SEM-EDX (a, b, e) and mapping images (Pt (c), C (d)) of Pt/CNT catalyst.

**Table 1** Atomic element composition of Pt/CNT catalyst.

| Element | Weight % | Atomic % |
|---|---|---|
| C | 87.75 | 93.66 |
| O | 7.52 | 6.02 |
| Pt | 4.73 | 0.31 |

TEM examined the morphology of the Pt/CNT catalyst. Figure 3 shows pictures of Pt/CNT in TEM with a particle-size histogram. Measurements were taken at 100, 200, and 500 nm for the Pt/CNT catalyst, respectively. The diagram shows that the metals were observed to be evenly distributed on the CNT surface. For the Pt/CNT catalyst, the average fleck size obtained using ImageJ software was 13 nm.

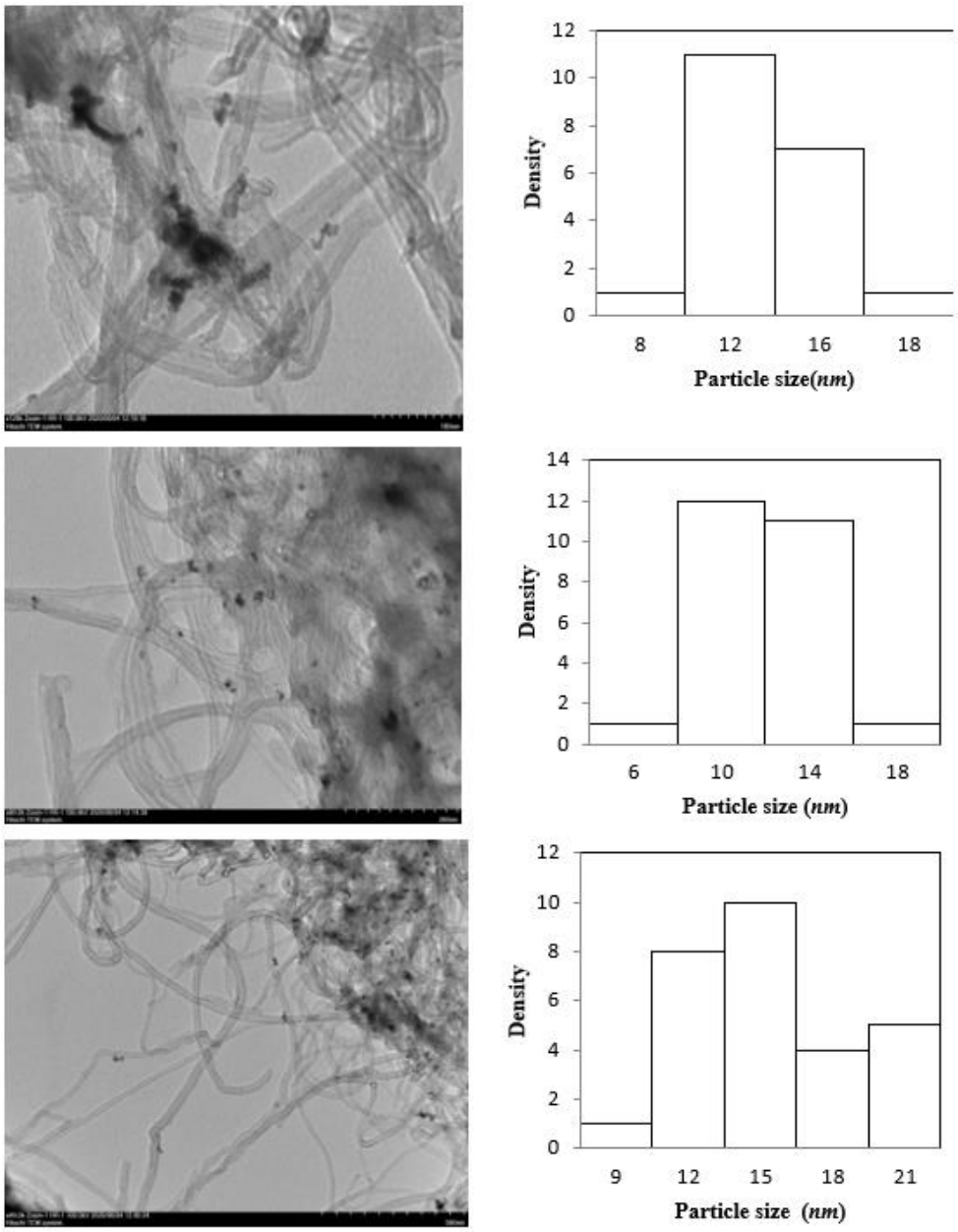


**Figure 3** TEM images and particle size of the Pt/CNT catalyst.

### *3.2 Hydrolysis Experiments of Pt/CNT Catalyst*

Hydrolysis tests were carried out at 30°C with 50 mg of Pt/CNT catalyst in 0.26 M sodium borohydride solution to study the hydrogen generation rate of carbon nanotube-supported Pt catalyst at different atomic ratios (0.5 percent, 1 percent, 7%, 10%, and 20%). The resulting hydrogen gas was collected in a gas burette using a water trap. Volumes of hydrogen gas were recorded at specified time intervals. Hydrogen production rates obtained using different ratios of Pt catalyst supported by carbon nanotubes are given in Figure 4. Although the initial rate of 20% Pt/CNT catalyst is higher than the initial rate of 7% Pt/CNT catalyst in the graph, 7% Pt/CNT is preferred. In addition, the 7% Pt catalyst showed better catalytic activity than the 10% Pt catalyst because one study aims to synthesize catalysts by reducing the use of precious noble metals.

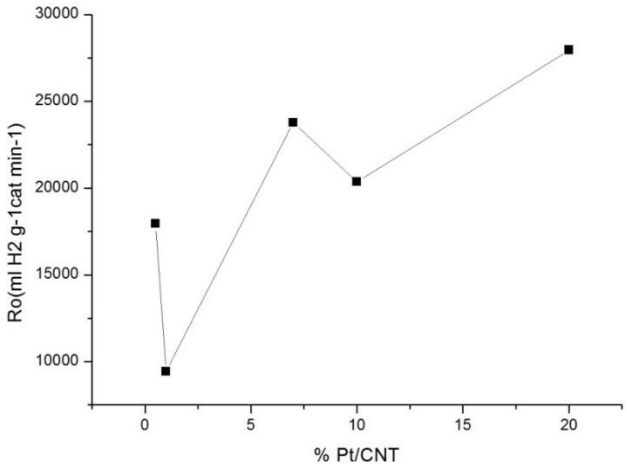


**Figure 4** Graph of initial rate depending on different rates of Pt loading to the CNT.

The pace at which the reaction proceeds can be represented as catalytic activity. In general, as the temperature rises, so does activity. Other reaction variables, on the other hand, have an impact on the reaction rate. As a result, the effects of several parameters on the reaction rate, such as NaOH mass, $NaBH_4$ mass, and catalyst quantity, were examined.

3.2.1 Sodium Hydroxide Concentration Effect

To study the effect of sodium hydroxide mass on the pace of hydrogen generation, hydrolysis tests were carried out at 30°C in the presence of 50 mg of 7% Pt/CNT catalyst in 0.26 M sodium borohydride solution and at various sodium hydroxide (NaOH) concentrations (0 percent, 1 percent, 3 percent and 5 percent by weight). The time-dependent graph of hydrogen production in the 0-5% NaOH concentration range is given in Figure 5. As shown in the figure, hydrogen generation decreases as the NaOH concentration increases. Despite this reduction, we used 1% by weight of NaOH in the experiments. The main reason for this is that NaOH prevents the self-hydrolysis of $NaBH_4$. Efficacy experiments affecting hydrolysis were performed in the presence of 1% NaOH concentration.

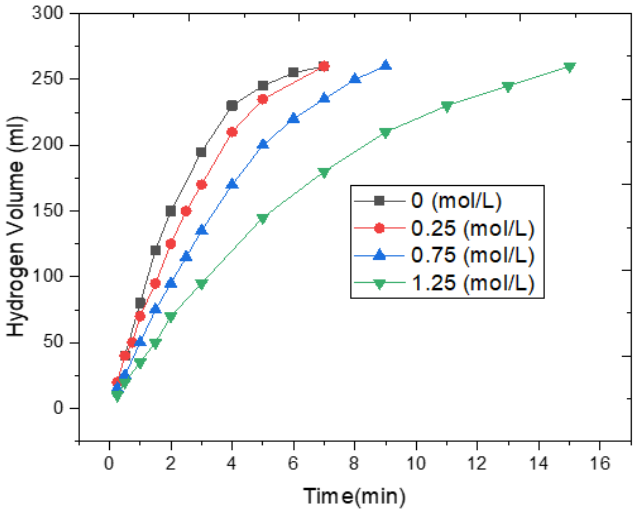


**Figure 5** Effect of NaOH concentration on hydrogen generation from $NaBH_4$ with 7% Pt/CNT catalyst.

### 3.2.2 Sodium Borohydride Concentration Effect

The graph of the variation of hydrogen volume amounts of different sodium borohydride concentrations with time is shown in Figure 6. The amount of hydrogen produced was determined at 30°C in the presence of 50 mg of 7% Pt/CNT catalyst using 1% NaOH solution and $NaBH_4$ (1%, 2%, 2.5%, 3% by weight) solution in the presence of 50 mg of 7% Pt/CNT catalyst. In trials conducted in the 0.26-0.80 M $NaBH_4$ solution, the amount of hydrogen obtained changed directly to the amount of sodium borohydride. A higher concentration of $NaBH_4$ in the system suggests a hydrogen source in the solution or a more significant concentration of sodium and borohydride ions in the solution. The reaction rate concerning NaBH4 depends on the reactivity between the borohydride ions and the catalyst's surface [46, 47].

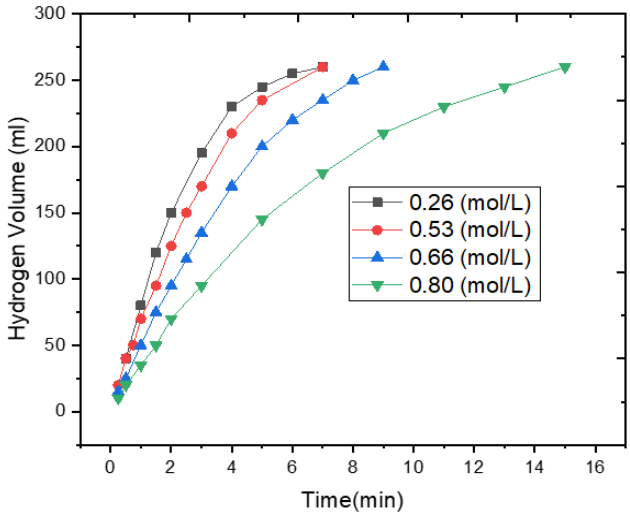


**Figure 6** Effect of $NaBH_4$ concentration on hydrogen generation from $NaBH_4$ with 7% Pt/CNT catalyst.

### 3.2.3 Catalyst Amount Effect

Hydrolysis tests were carried out at 30°C using a 1% NaOH solution and a 0.26 M $NaBH_4$ solution to investigate the influence of catalyst quantity on hydrogen efficiency. The graph of the change of hydrogen volumes over time in the presence of 10-75 mg of 7% Pt/CNT catalyst is shown in Figure 7. The time it took for the hydrolysis reaction to complete decreased as the amount of catalyst grew, as shown in the graph. The hydrolysis of sodium borohydride can be said to be a catalyst-controlled reaction [48]. Without the catalyst, the process slows down and eventually stops. The increase in the reaction rate here is that the active sites of the catalyst increase in direct proportion to the amount of catalyst. Therefore, the adsorption time of sodium borohydride on the catalyst surface decreased further as the amount of catalyst in the environment increased, thus reducing the completion time of the reaction. As seen in Figure 7, the hydrolysis reaction is completed in 25 minutes in the presence of 25 mg of 7% Pt/CNT catalyst, while the hydrolysis reaction is completed in 7 minutes in the presence of 50 mg of 7% Pt/CNT catalyst under the same parameters. As a result, the increase in the amount of catalyst increases the activity of the catalyst.

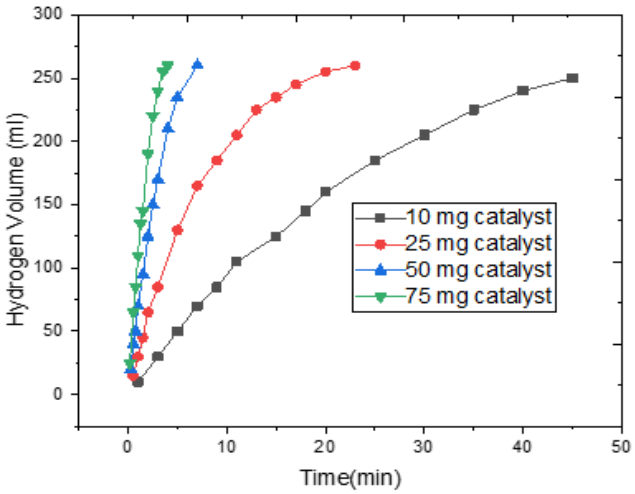


**Figure 7** Effect of catalyst amount on hydrogen production rate from $NaBH_4$ with 7% Pt/CNT.

3.2.4 Temperature Effect

Hydrolysis tests were carried out using 1% NaOH and 0.26 M $NaBH_4$ solutions in the presence of 50 mg of 7% Pt/CNT catalyst in the temperature range of 20-50°C to investigate the influence of temperature on the amount of hydrogen produced. The graph of the obtained hydrogen volumes over time is given in Figure 8. The time it took for the hydrolysis reaction to complete decreased as the temperature rose, as expected. While the hydrolysis reaction takes 15 minutes at 20°C, it only takes 5 minutes at 40°C under the same conditions, as shown in the graph. When the temperature of the reaction medium is doubled, the hydrolysis reaction takes three times less time to complete.

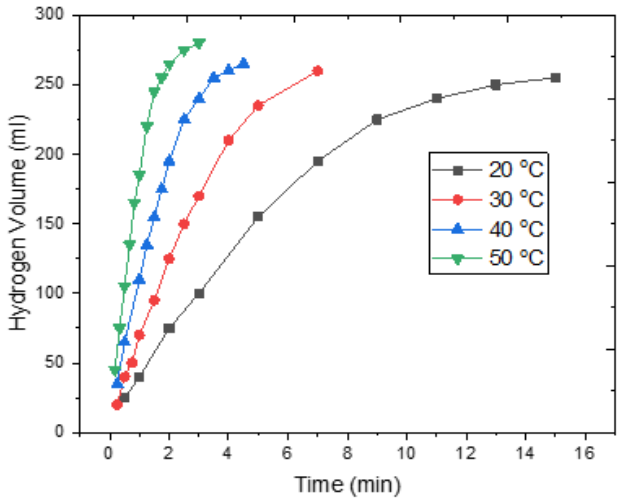


**Figure 8** Effect of temperature on hydrogen generation from $NaBH_4$ with 7% Pt/CNT catalyst.

To examine the active cycle stability of the catalysts, hydrolysis experiments were performed using 1% NaOH solution and 0.26 M $NaBH_4$ solution at 30°C. The 7% Pt/CNT catalyst used in the hydrolysis experiments was washed, filtered, and used again. The graph of the change in hydrogen volumes of the catalyst used 5 times in a row over time is shown in Figure 9. The figure shows that

100% hydrogen production from $NaBH_4$ is achieved even though the catalyst is used 5 times. In other words, complete transformation is achieved. As full conversion is achieved, reaction time increases. This is due to the decrease in the active sites' activity on the catalyst's surface after washing and reuse. Additionally, the increased concentration of metaborate during the hydrolysis of NaBH4 with a deactivation effect and the increased viscosity of the solution may also cause a decrease in catalytic performance [49].

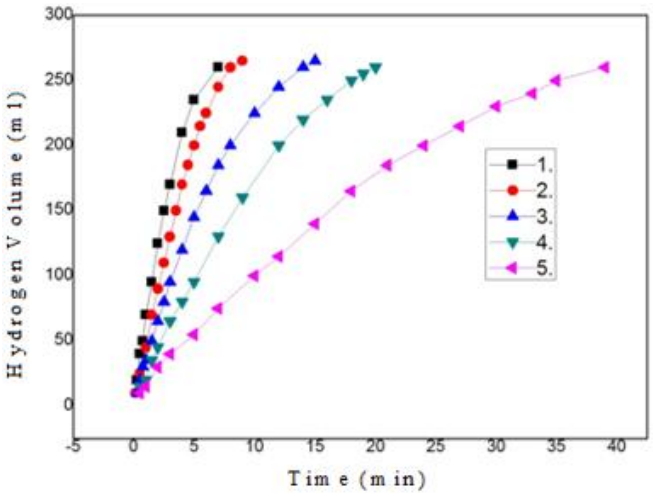


**Figure 9** The active cycle stability of the catalyst.

Calculation of activation energy and reaction order: As stated in the literature, k values were calculated at different temperatures [25, 31, 32]. The reaction order n was estimated as 0.8, which aligns with the data obtained. The activation energy of 7% Pt/CNT catalyst was calculated as *Ea = (5311,9·8,314)/1000 = 44,16314 kj/mol.* The Arrhenius plot for different temperature values and reaction rate constants (k) is given in Figure 10.

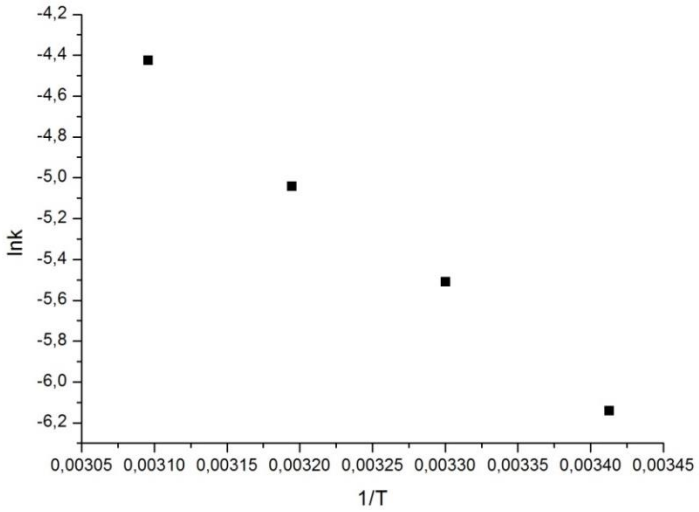


**Figure 10** lnk - 1/T Arrhenius plot of 7% Pt/CNT catalyst.

### *3.3 Investigation of Supercapacitor Property of Pt/CNT Catalyst*

3.3.1 Cyclic Voltammetry (CV)

The current was measured and graphed at several fixed scanning rates (10, 25, 50, 75, 100, 150, 200, 250 mV) by applying voltage to the cell. Obtained current-potential graphs are given in Figure 11 and Figure 12. As seen in Figure 12, the cyclic curves close to the parallelogram for a successful supercapacitor at high sweep rates (100, 150, 200, 250 mV/s). As shown in Figure 11, cyclic curves at low scanning speeds (10, 25, 50, 75) may deviate from the symmetry that provides this parallelogram. In particular, the cyclic curve formed at a scanning speed of 10 mV/s moves away from the parallelogram appearance. The electrode material in which the stored charges are distributed is related to the ohmic resistance (IR drop) created against the movement of the electrolyte in the nano-hollow carbon matrix, which is the reason for this (EDLC) production mechanism.

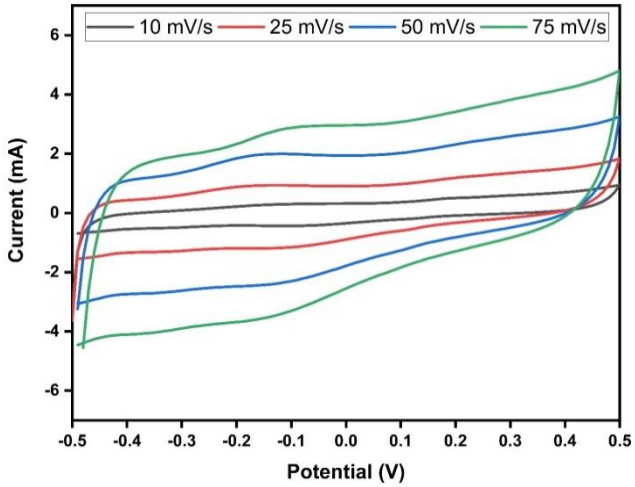


**Figure 11** Cyclic curves of the 7% Pt/CNT electrode at low scan rates.

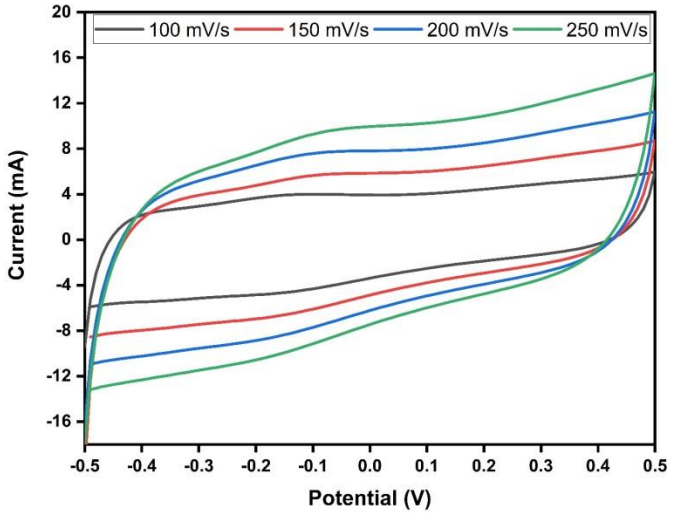


**Figure 12** Cyclic curves of the 7% Pt/CNT electrode at high scan rates.

### 3.3.2 Electrochemical Impedance Spectroscopy (EIS)

Electrochemical impedance is measured from the current signal formed in the system against the potential applied to the system. Graphs were drawn as Nyquist curves from the signal data, and the resistance properties were interpreted in these graphs. The resulting graphic is given in Figure 13. For the Nyquist curve, the slope angle was 79° at low-frequency values. The mid-frequency region's load transfer resistance (Rct) is 4 Ω, and the equivalent series resistance is 0.12 Ω. Supercapacitors' series resistance (Resr) creates voltage drops across the device. Because of the low resistance value of the electron and the resulting low voltage drops in energy transmission, it can be stated that the prepared electrode will play an essential role in energy storage [50].

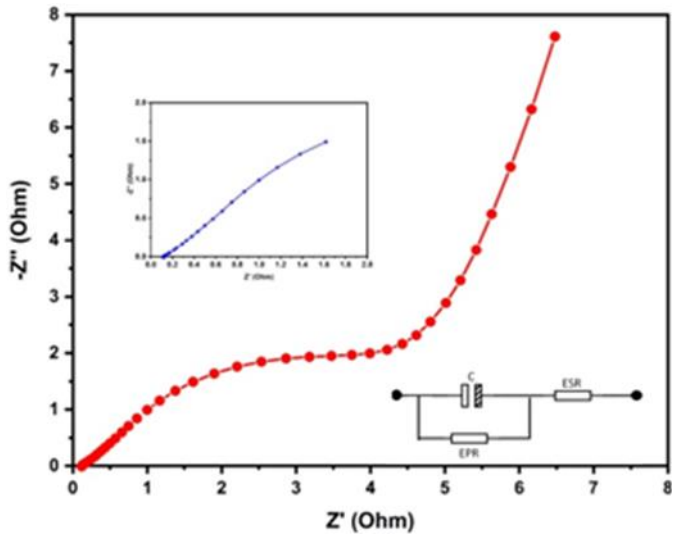


**Figure 13** Nyquist plot and the equivalent circuit model of the 7% Pt/CNT supercapacitor.

### 3.3.3 Galvanostatic Charge-Discharge (GCD)

The fluctuation of the cell throughout a specific potential range was observed over time at a constant current density (usually 1 A/g). The performance of the produced catalyst sample at different constant current densities (1.00, 1.25, 1.50, 1.75, and 2.0 A/g) was measured for both electrolytes. The resulting graph is given in Figure 14. The fact that the GCD curve formed during the charge-discharge of a supercapacitor is in the form of an isosceles triangle indicates that the device works ideally and reversibly. The figure shows that the GCD graph obtained for the electrode prepared using 7% Pt/CNT catalyst showed ideal supercapacitor behavior. According to the GCD curves' discharge times, the supercapacitor cells' specific capacitances were calculated according to Equation 2.5. Calculated capacitance values and IR drop values are given in Table 2.

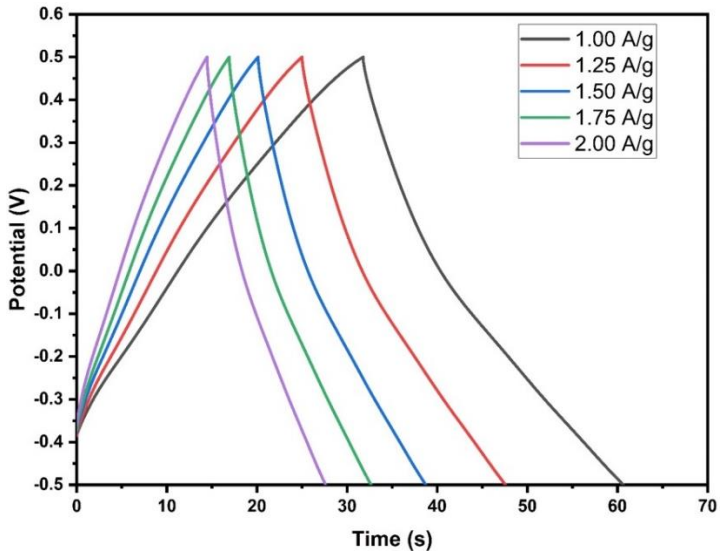


**Figure 14** Charge-discharge graph of the cell at different current densities.

**Table 2** Capacitance and IR drop at different current densities.

| Current density (A/g) | Specific capacitance (F/g) | IR drop (mV) |
|---|---|---|
| 1.00 | 57.78 | 7 |
| 1.25 | 56.45 | 8 |
| 1.50 | 55.80 | 10 |
| 1.75 | 55.10 | 11 |
| 2.00 | 52.60 | 14 |

A comparison of the capacities of Pt-based catalysts used in supercapacitor applications is given in Table 3. In most of the literature studies, Pt metal was used in catalyst synthesis at a rate of 10% to 20%. In addition, a second metal was added to the support material, and activation processes were carried out. Considering all these, it can be said that the performance of the 7% Pt/CNT catalyst used in this study is suitable as a supercapacitor electrode material.

**Table 3** Comparison of some Pt-based supercapacitor electrode catalysts in the literature.

| Catalyst | Current Density (A/g) | Capacitance (F/g) | Reference |
|---|---|---|---|
| PtNWs/CS-900 | 1 | 231 | [51] |
| PtNWs/CS-700 | 1 | 120 | [51] |
| $Pt/MnO_2/C_3N_4$ | 0.1 | 577.10 | [52] |
| $ZnFe_2O_4$-$ZrO_2$/Pt | 1 | 194.25 | [53] |
| Pt/MiCF-60 | 1 | 100 | [54] |
| Pt/CNT | 1 | 57.78 | This work |

The loop-dependent capacitance graph is given in Figure 15. The figure shows that the capacitance reduction is 6.4% at the end of 120 cycles. In other words, the supercapacitor continues to operate with 93.6% efficiency.

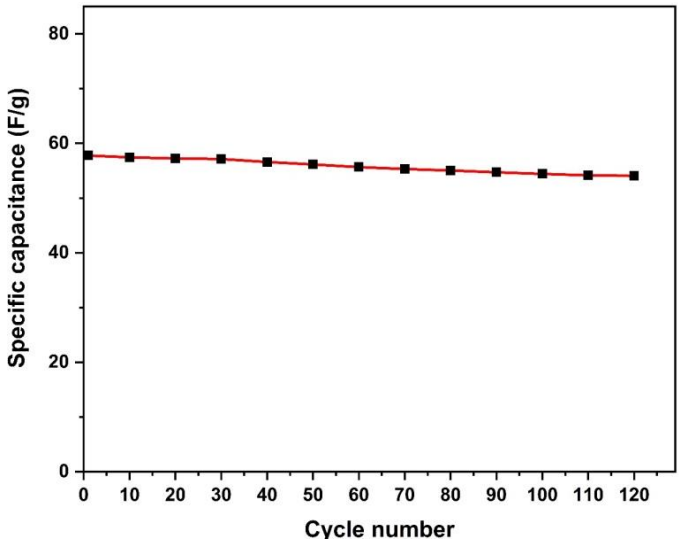


**Figure 15** Graph of capacitance by number of cycles.

When the Energy and Power densities are calculated for 1 A/g current densities,

E = 8,025 Wh/kg

P = 963 W/kg was found as.

According to the Ragone graph [55] for various energy storage and conversion devices, the obtained supercapacitor electrode material shows ideal supercapacitor properties.

## 4. Conclusions

This research demonstrates how raw materials can be used to create high-performance bifunctional materials such as hydrolysis catalysts and supercapacitor electrodes to develop renewable energy storage and conversion devices. As a result of the hydrolysis experiments, the activation energy of the 7% Pt/CNT catalyst was found to be 44,163 kj/mol with an initial rate of 21949,69 $mlH_2g_{cat}min^{-1}$. As a result of electrochemical measurements, the specific capacitance of 7% Pt/CNT electrode material was found to be 57.78 F/g. Energy and power density were calculated as 8,025 Wh/kg and 963 W/kg, respectively. The electrodes subjected to the stability test showed only a 6.4% capacitance reduction. Electrodes prepared in the light of the obtained data are considered promising in energy storage due to their low internal resistance and stability.

Consequently, a dual-functional material was used as a hybrid energy source that is both a catalyst for hydrogen generation and an electrode material for the supercapacitor simultaneously. So we can call this catalyst “cap-cat”. The catalyst used in this study is promising for this recently studied topic.

## Acknowledgments

Author wishes to thank Prof. Dr. Ömer ŞAHİN and Prof. Dr. Hilal DEMİR KIVRAK for providing advice, scientific help and technical support.

## Author Contributions

The author did all the research work of this study.

## Competing Interests

The author has declared that no competing interests exist.

## References


1. ATELGE R. Türkiye'de Sığır Gübresinden Biyoyakıt Olarak Biyogaz Üretiminin Potansiyeli ve 2030 ve 2053 Yıllarında Karbon Emisyonlarının Azaltılmasına Öngörülen Etkisi. Int J Innov Eng Appl. 2021; 5: 56-64.
2. ATELGE R. Kısmi Yük Koşullarında Dizel-Biyogaz Kullanılarak Çift Yakıtlı Dizel Motorun Enerji ve Ekserji Analizi. Avrupa Bilim ve Teknoloji Dergisi. 2021; 334-346. doi: doi.org/10.31590/ejosat.961833.
3. Akdemir M, Hansu F. Effect of induction heating aided dielectric barrier discharge on the elimination of $SO_2$, $NO_X$, and CO Gases. Water Air Soil Pollut. 2020; 231: 14.
4. Wei Y, Wang Y, Wei L, Zhao X, Zhou X, Liu H. Highly efficient and reactivated electrocatalyst of ruthenium electrodeposited on nickel foam for hydrogen evolution from $NaBH_4$ alkaline solution. Int J Hydrogen Energy. 2018; 43: 592-600.
5. Guo J, Hou Y, Li B, Liu Y. Novel Ni-Co-B hollow nanospheres promote hydrogen generation from the hydrolysis of sodium borohydride. Int J Hydrogen Energy. 2018; 43: 15245-15254.
6. Duman F, Atelge MR, Kaya M, Atabani AE, Kumar G, Sahin U, et al. A novel Microcystis aeruginosa supported manganese catalyst for hydrogen generation through methanolysis of sodium borohydride. Int J Hydrogen Energy. 2020; 45: 12755-12765.
7. Kaya M, Atelge MR, Bekirogullari M, Eskicioglu C, Atabani AE, Kumar G, et al. Carbon molecular sieve production from defatted spent coffee ground using $ZnCl_2$ and benzene for gas purification. Fuel. 2020; 277: 118183.
8. Ozarslan S, Atelge MR, Kaya M, Ünalan S. Evaluation of tea factory wastes in energy and other areas: A review. Energy Environ Storage. 2021; 35-44. doi: 1052924/QMDG6303.
9. Akdemir M, Avci Hansu T, Caglar A, Kaya M, Demir Kivrak H. Ruthenium modified defatted spent coffee catalysts for supercapacitor and methanolysis application. Energy Storage. 2021; 3: e243.
10. Karuppasamy M, Muthu D, Haldorai Y, Rajendra Kumar RT. Solvothermal synthesis of $Fe_3S_4$@ graphene composite electrode materials for energy storage. Carbon Lett. 2020; 30: 667-673.
11. Cho SD, Lee SY, Hyun JG, Paik KW. Comparison of theoretical predictions and experimental values of the dielectric constant of epoxy/$BaTiO_3$ composite embedded capacitor films. J Mater Sci Mater Electron. 2005; 16: 77-84.
12. Béguin F, Presser V, Balducci A, Frackowiak E. Supercapacitors: Carbons and electrolytes for advanced supercapacitors (Adv. Mater. 14/2014). Adv Mater. 2014; 26: 2283.
13. Sun H, He W, Zong C, Lu L. Template-free synthesis of renewable macroporous carbon via yeast cells for high-performance supercapacitor electrode materials. ACS Appl Mater Interfaces. 2013; 5: 2261-2268.
14. Dubey R, Guruviah V. Review of carbon-based electrode materials for supercapacitor energy storage. Ionics. 2019; 25: 1419-1445.
15. Gao Z, Ding C, Wang J, Ding G, Xue Y, Zhang Y, et al. Cobalt nanoparticles packaged into nitrogen-doped porous carbon derived from metal-organic framework nanocrystals for hydrogen production by hydrolysis of sodium borohydride. Int J Hydrogen Energy. 2019; 44: 8365-8375.

16. Borgschulte A, Jain A, Ramirez-Cuesta AJ, Martelli P, Remhof A, Friedrichs O, et al. Mobility and dynamics in the complex hydrides $LiAlH_4$ and $LiBH_4$. Faraday Discuss. 2011; 151: 213-230.
17. Xu Y, Wu C, Chen Y, Huang Z, Luo L, Wu H, et al. Hydrogen generation behaviors of $NaBH_4$-$NH_3BH_3$ composite by hydrolysis. J Power Sources. 2014; 261: 7-13.
18. Bozkurt G, Özer A, Yurtcan AB. Development of effective catalysts for hydrogen generation from sodium borohydride: Ru, Pt, Pd nanoparticles supported on $Co_3O_4$. Energy. 2019; 180: 702-713.
19. Uzundurukan A, Devrim Y. Hydrogen generation from sodium borohydride hydrolysis by multi-walled carbon nanotube supported platinum catalyst: A kinetic study. Int J Hydrogen Energy. 2019; 44: 17586-17594.
20. Hansu F. The effect of dielectric barrier discharge cold plasmas on the electrochemical activity of Co-Cr-B based catalysts. J Energy Inst. 2015; 88: 266-274.
21. Kaya M. Production of metal-free catalyst from defatted spent coffee ground for hydrogen generation by sodium borohyride methanolysis. Int J Hydrogen Energy. 2020; 45: 12731-12742.
22. Kaya M. Evaluating organic waste sources (spent coffee ground) as metal-free catalyst for hydrogen generation by the methanolysis of sodium borohydride. Int J Hydrogen Energy. 2020; 45: 12743-12754.
23. Bekirogullari M. Hydrogen production from sodium borohydride by $ZnCl_2$ treated defatted spent coffee ground catalyst. Int J Hydrogen Energy. 2020; 45: 9733-9743.
24. Bekirogullari M, Abut S, Duman F, Hansu TA. Lake sediment based catalyst for hydrogen generation via methanolysis of sodium borohydride: An optimization study with artificial neural network modelling. React Kinet Mech Catal. 2021; 134: 57-74.
25. Avci Hansu T, Caglar A, Demir Kivrak H, Sahin O. Structure of ruthenium nanocatalysts of bismuth, investigation of its effect on hydrolysis performance and kinetic studies. Energy Storage. 2021; 3: e267.
26. Hansu TA, Caglar A, Sahin O, Kivrak H. Hydrolysis and electrooxidation of sodium borohydride on novel CNT supported CoBi fuel cell catalyst. Mater Chem Phys. 2020; 239: 122031.
27. Hansu TA, Çaglar A, Sahin O, Kivrak H. A comparative study for sodium borohydride dehydrogenation and electrooxidation on cerium and cobalt catalysts. Int J Ecosyst Ecol Sci. 2020; 10: 389.
28. Özarslan S, Atelge MR, Kaya M, Ünalan S. Production of dual functional carbon material from biomass treated with NaOH for supercapacitor and catalyst. Energy Storage. 2021; 3: e257.
29. Karakaş DE, Akdemir M, Atelge MR, Kaya M, Atabani AE. Defatted spent coffee grounds-supported cobalt catalyst as a promising supercapacitor electrode for hydrogen production and energy storage. Clean Technol Environ Policy. 2021; 25: 483-493.
30. Akdemir M, Imanova G, Karakaş DE, Kıvrak HD, Kaya M. High efficiency biomass-based metal-free catalyst as a promising supercapacitor electrode for energy storage. Available at SSRN 3908407. 2021. Available from: https://papers.ssrn.com/sol3/papers.cfm?abstract_id=3908407.
31. Avci Hansu T, Sahin O, Çağlar A, Demir Kivrak H. Untangling the cobalt promotion role for ruthenium in sodium borohydride dehydrogenation with multiwalled carbon nanotube-supported binary ruthenium cobalt catalyst. Int J Energy Res. 2021; 45: 6054-6066.
32. Avci Hansu T, Sahin O, Caglar A, Kivrak H. A remarkable Mo doped Ru catalyst for hydrogen generation from sodium borohydride: The effect of Mo addition and estimation of kinetic parameters. React Kinet Mech Catal. 2020; 131: 661-676.

33. KIVRAK HD, Caglar A, HANSU TA, ŞAHİN Ö. Carbon nanotube supported direct borohydride fuel cell anode catalysts: The effect of catalyst loading. MANAS J Eng. 2020; 8: 1-10.
34. Huff C, Biehler E, Quach Q, Long JM, Abdel-Fattah TM. Synthesis of highly dispersive platinum nanoparticles and their application in a hydrogen generation reaction. Colloids Surf A Physicochem Eng Asp. 2021; 610: 125734.
35. Junior IM, Sperandio GH, Moreira RP, Silva TA. Nanocarbon as catalyst support for fuel hydrogen generation by hydrolysis of sodium borohydride. In: NanoCarbon: A wonder material for energy applications: Volume 1: Basics to advanced applications for energy production. Singapore: Springer Nature Singapore; 2024. pp. 293-308.
36. Zhong CJ, Luo J, Njoki PN, Mott D, Wanjala B, Loukrakpam R, et al. Fuel cell technology: Nano-engineered multimetallic catalysts. Energy Environ Sci. 2008; 1: 454-466.
37. Noor T, Qi Y, Chen D. Hydrogen dependence of the reaction mechanism and kinetics of water gas shift reaction on Ni catalyst: Experimental and DFT study. Appl Catal B. 2020; 264: 118430.
38. Shao Y, Zhang S, Wang C, Nie Z, Liu J, Wang Y, et al. Highly durable graphene nanoplatelets supported Pt nanocatalysts for oxygen reduction. J Power Sources. 2010; 195: 4600-4605.
39. Çağlar A, Aldemir A, Kivrak H. Alcohol electrooxidation study on carbon nanotube supported monometallic, Pt, Bi, and Ru catalysts. Fullerenes Nanotubes Carbon Nanostruct. 2018; 26: 863-870.
40. Zhang D, Wu Y, Li T, Huang Y, Zhang A, Miao M. High performance carbon nanotube yarn supercapacitors with a surface-oxidized copper current collector. ACS Appl Mater Interfaces. 2015; 7: 25835-25842.
41. Es-Souni M, Schopf D. Modified nanocarbon surfaces for high performance supercapacitor and electrocatalysis applications. Chem Commun. 2015; 51: 13650-13653.
42. Tang H, Chen JH, Huang ZP, Wang DZ, Ren ZF, Nie LH, et al. High dispersion and electrocatalytic properties of platinum on well-aligned carbon nanotube arrays. Carbon. 2004; 42: 191-197.
43. Zhang LL, Zhao XS. Carbon-based materials as supercapacitor electrodes. Chem Soc Rev. 2009; 38: 2520-2531.
44. Zhong C, Deng Y, Hu W, Qiao J, Zhang L, Zhang J. A review of electrolyte materials and compositions for electrochemical supercapacitors. Chem Soc Rev. 2015; 44: 7484-7539.
45. Zhang B, Xue Y, Sun H, Jiang A, Li Z, Hao J. A green synthesis of “naked” Pt and PtPd catalysts for highly efficient methanol electrooxidation. RSC Adv. 2016; 6: 56083-56090.
46. Holbrook KA, Twist PJ. Hydrolysis of the borohydride ion catalysed by metal-boron alloys. J Chem Soc A. 1971. doi: 10.1039/J19710000890.
47. Zhuang DW, Kang Q, Muir SS, Yao X, Dai HB, Ma GL, et al. Evaluation of a cobalt-molybdenum-boron catalyst for hydrogen generation of alkaline sodium borohydride solution-aluminum powder system. J Power Sources. 2013; 224: 304-311.
48. Kim JH, Kim KT, Kang YM, Kim HS, Song MS, Lee YJ, et al. Study on degradation of filamentary Ni catalyst on hydrolysis of sodium borohydride. J Alloys Compd. 2004; 379: 222-227.
49. Chen B, Chen S, Bandal HA, Appiah-Ntiamoah R, Jadhav AR, Kim H. Cobalt nanoparticles supported on magnetic core-shell structured carbon as a highly efficient catalyst for hydrogen generation from $NaBH_4$ hydrolysis. Int J Hydrogen Energy. 2018; 43: 9296-9306.
50. Akdemir M. Investigation of co-doped chlorella vulgaris as a supercapacitor electrode for energy storage. J Mater Sci Mater Electron. 2021; 32: 27243-27250.

51. Fan Y, Liu PF, Yang ZJ, Jiang TW, Yao KL, Han R, et al. Bi-functional porous carbon spheres derived from pectin as electrode material for supercapacitors and support material for Pt nanowires towards electrocatalytic methanol and ethanol oxidation. Electrochim Acta. 2015; 163: 140-148.
52. Yousaf AB, Khan R, Imran M, Fasehullah M, Zeb A, Zaidi SJ, et al. Carbon nitride embedded $MnO_2$ nanospheres decorated with low-content Pt nanoparticles as highly efficient and durable electrode material for solid state supercapacitors. J Electroanal Chem. 2017; 801: 84-91.
53. Jinxi W, Aimin W, Ghasemi AK, Lashkenari MS, Pashai E, Karaman C, et al. Tailoring of $ZnFe_2O_4$-$ZrO_2$-based nanoarchitectures catalyst for supercapacitor electrode material and methanol oxidation reaction. Fuel. 2023; 334: 126685.
54. Liu Z, Fu D, Liu F, Han G, Liu C, Chang Y, et al. Mesoporous carbon nanofibers with large cage-like pores activated by tin dioxide and their use in supercapacitor and catalyst support. Carbon. 2014; 70: 295-307.
55. Kötz R, Carlen MJ. Principles and applications of electrochemical capacitors. Electrochim Acta. 2000; 45: 2483-2498.